Kinetic neutron diffraction study of Nb_3Sn phase formation in superconducting wires

2006 J. Phys.: Condens. Matter 18 1449

(http://iopscience.iop.org/0953-8984/18/4/028)

INSTITUTE OF PHYSICS PUBLISHING JOURNAL OF PHYSICS: CONDENSED MATTER

J. Phys.: Condens. Matter **18** (2006) 1449–1457 doi:10.1088/0953-8984/18/4/028

Kinetic neutron diffraction study of Nb_3Sn phase formation in superconducting wires

M Al-Jawad[1], P Manuel[2], C Ritter[3] and S H Kilcoyne[4]

[1] School of Physics and Astronomy, University of Leeds, Leeds LS2 9JT, UK
[2] ISIS Facility, Rutherford Appleton Laboratory, Didcot, Oxfordshire OX11 0QX, UK
[3] Institut Laue Langevin, Grenoble, France
[4] Institute of Materials Research, University of Salford, Salford, M5 4WT, UK

E-mail: m.al-jawad@leeds.ac.uk

Received 31 October 2005
Published 13 January 2006
Online at stacks.iop.org/JPhysCM/18/1449

Abstract

The kinetics of Nb_3Sn phase formation in commercial multifilamentary wires have been studied as a function of time and temperature using time-resolved, *in situ* neutron diffraction. This work shows that at higher temperatures the Nb_3Sn phase forms in a fraction of the recommended annealing time. A temperature-independent Avrami exponent of $n = 0.51 \pm 0.01$ was observed, indicating a diffusion-controlled growth mechanism, and a large apparent activation energy of $E_a = 10 \pm 1$ eV is reported where the energies of nucleation and growth both contribute.

1. Introduction

There is high demand for specialist high-field magnets (>8 T), which has resulted in the development of a multi-million dollar industry dedicated to magnet design and production. Nb_3Sn and NbTi are the most widely used materials for high-field superconducting magnets, primarily due to the relatively low cost of raw materials and processing. Unlike NbTi, Nb_3Sn is extremely brittle, and it is not possible to wind Nb_3Sn wires into a coil or solenoid. Instead, Cu sheathed Nb and Sn wires are drawn, wound to the desired size and shape, and then heated to promote the reaction of Nb with Sn to form the Nb_3Sn phase. All standard multifilamentary Nb_3Sn wires include substantial amounts of Cu to electromagnetically stabilize and protect the superconductor. The Cu also acts as a thermal stabilizer whilst the wires are in use, assisting in the rapid transfer of heat from the superconducting filaments to the surrounding coolant. Several heat treatments have been proposed for the formation of high quality Nb_3Sn from precursor Nb–Sn–Cu wires. Despite their differences all treatments are time consuming, each taking ∼300 h (13 days) to complete.

In this paper we have studied and characterized a three-stage heat treatment used by Oxford Instruments Superconductivity (OIS) in the production of superconducting Nb_3Sn magnets. Stage 1 is an isothermal anneal at ∼210 °C for approximately 65 h. This stage facilitates

the production of α-, η-, and ε-bronze phases (CuSn solid solution, Cu_6Sn_5, and Cu_3Sn respectively). Nb_3Sn forms more readily by solid-state diffusion from Cu–Sn bronzes than by reaction with molten tin, therefore it is important to have a low temperature annealing stage below the melting point of Sn (227 °C) to allow formation of Cu–Sn bronzes. Stage 2 is an isothermal anneal at ∼340 °C for ∼50 h. During this stage the low melting point bronzes are converted into high melting point bronze phases. Nb_3Sn is formed during the third and final stage, which takes place at ∼650 °C for 160–180 h. During this anneal Sn diffuses out of the bronze phases into the Nb filaments to form Nb_3Sn via a solid-state reaction. The time spent at, and temperature of, this stage can affect the critical current of the final superconducting wires by influencing the fraction of Nb_3Sn phase formed, the stoichiometry of the Nb_3Sn phase, and the grain size. The optimum temperature is one that minimizes the Nb_3Sn grain size and maximizes the critical current density, whilst maximizing the amount of Nb_3Sn phase formed. As a result there is some debate over the temperature of the final stage anneal.

Most studies into the effect of heat treatment on the production and overall performance of Nb_3Sn composites have involved annealing material at a particular temperature then quenching and analysing the sample at room temperature. The majority of information about the crystallography and microstructure of the Nb–Sn–Cu system has been obtained in this way. Investigations using techniques such as scanning electron microscopy (SEM) [1–6], transmission electron microscopy [7], laboratory x-ray diffraction measurements [8], and energy dispersive x-ray spectroscopy [9, 10] have also all used the heat and quench method to analyse heat-treated samples.

In this paper we explore the crystallographic and microstructural characteristics of Nb_3Sn wires during heat treatment *in situ* using kinetic neutron diffraction. The benefits of using neutron diffraction to study the crystallographic and microstructural properties of phases in Nb–Sn–Cu wires are twofold: firstly measurements can be made in a matter of minutes, thereby providing information on the kinetics of phase growth within the wires, and secondly wires can be studied in bulk, thus avoiding the problems of statistical variations encountered when studying very small samples.

2. Isothermal phase transformations

A model to describe isothermal phase formation and transformation was developed by Kolmogorov [11], Johnson and Mehl [12] and Avrami [13–15]. This model (commonly referred to as the JMAK model) is now widely accepted and is used to describe the crystallization of amorphous materials [16] and crystalline to crystalline phase transformations [17]. In the JMAK model the time dependence of the crystalline volume fraction $V_T(t)$ follows the Avrami equation:

$$V_T(t) = 1 - \exp\left(-\left(\frac{t}{\tau}\right)^n\right) \tag{1}$$

where V_T is the fraction of volume transformed, τ is the inverse rate constant which represents the time constant for phase formation and n is the Avrami exponent. For a three-dimensional nucleation and growth process n will have a value between 3 and 4. In the initial JMAK model certain assumptions are made: (1) the sample is of infinite size and boundary effects can be ignored, (2) the nucleation sites are randomly distributed and nucleation occurs at a constant rate, and (3) grain growth continues until impingement occurs. This model has been modified to describe the kinetics of a reaction in which the growth process is controlled by a diffusion process [18]. For a diffusion controlled reaction V_T is no longer defined as the fraction of the whole assembly which has transformed, but instead is defined as the volume fraction of an

individual phase in the whole assembly. In this model n takes values from 0.5 to >2, where, for example, $n = 0.5$ represents the thickening of large plate-like crystals and $n = 1$ is obtained for needle-like crystals. A more complete description of the Avrami equation for diffusion controlled processes and a table listing the values of n, which may be obtained in the modified model, can be found in *The Theory of Transformations in Metals and Alloys* by Christian [18].

A more useful form of the JMAK equation is the linearized form which is obtained by taking the double natural logarithm of both sides to give

$$\ln \ln \left(\frac{1}{1 - V_T} \right) = n \ln \left(\frac{t}{\tau} \right). \tag{2}$$

Plots of $\ln \ln(1/1 - V_T)$ versus $\ln(t/\tau)$ should be a straight line a gradient of n.

The activation energy of the growth process, E_a, and its associated attempt frequency, k_o, can be determined if we assume that the rate constants follow the Arrhenius law:

$$k = k_o \exp - \left(\frac{E_a}{k_B T} \right) \tag{3}$$

where $k(=1/\tau)$ is the rate constant, k_B is Boltzmann's constant, and T is the absolute temperature. A plot of $\ln k$ versus $1/k_B T$ gives a straight line from which E_a and k_o can be determined.

3. Experimental procedure

Three samples of 5 m lengths of Nb–Sn–Cu precursor wire (weighing approximately 6 g each) were sealed in separate silica tubes and annealed in a standard carbolite furnace at 210 °C for 65 h. The furnace temperature was then increased at a rate of 50 °C h^{-1} to 340 °C and the samples were annealed for a further 50 h. The three silica tubes were removed at the same time and the wires were water quenched. These heat treatments follow stages 1 and 2 of the OIS recommendations. Note that the Nb_3Sn phase only starts to form above 550 °C, therefore it is assumed that quenching the wires at 340 °C will not affect the Nb_3Sn phase formation stage.

Neutron diffraction patterns were collected on the D20 diffractometer at the Institut Laue Langevin in Grenoble. Each sample of partially reacted wire (∼6 g) was loaded in turn into a cylindrical 8 mm diameter vanadium sample holder. This was mounted in the standard vanadium-element vacuum furnace and placed in the neutron beam. D20 was used in its high resolution set-up with a Ge(113) monochromator providing neutrons of wavelength $\lambda = 1.9$ Å. The formation of Nb_3Sn was examined in detail during isothermal annealing at three different temperatures: 660, 675, and 700 °C. For each specimen, spectra were collected at room temperature, and then at five minute intervals during annealing at 700 °C, and every two minutes when annealing at 660 and 675 °C.

The rate of Nb_3Sn phase formation was determined via full Rietveld refinement of the diffraction patterns using the General Structure Analysis System (GSAS) [19].

4. Results and discussion

4.1. Influence of temperature–time heat treatment profile on Nb_3Sn phase formation

Figure 1 shows a section of the neutron thermogram collected during the anneal at 660 °C. Similar thermograms were collected at 675 and 700 °C. At all temperatures the Bragg peaks arising from the Nb_3Sn phase ($2\theta = 41.8°$, 47.0°, and 51.8°) sharpen and grow during the period of the anneal, while the intensities of the Nb ($2\theta = 47.7°$) and α-bronze peaks ($2\theta = 52.6°$) decrease.

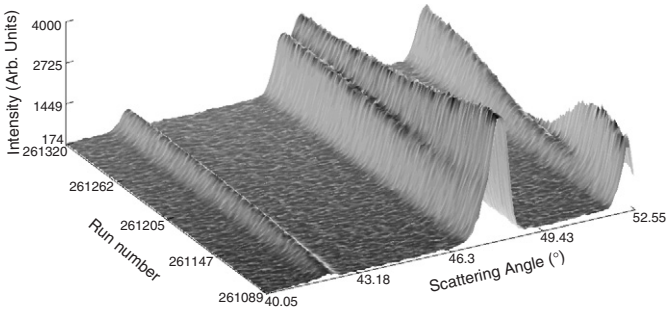

Figure 1. A section of the neutron thermogram collected on D20 whilst annealing at 660 °C for ∼7 h. Data were collected for two minutes per scan. Nb_3Sn Bragg peaks at $2\theta = 41.8°$, 47.0°, and 51.8°, Nb at $2\theta = 47.7°$ and α-bronze peak at $2\theta = 52.6°$.

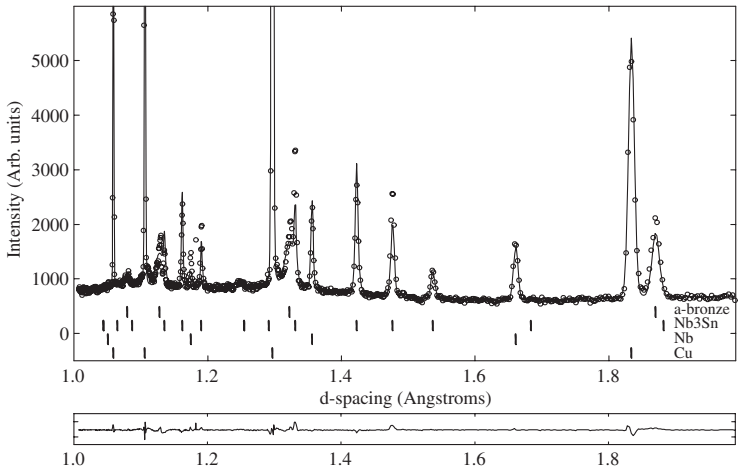

Figure 2. A typical neutron powder diffraction pattern of a Nb–Sn–Cu wire sample. The pattern was collected after annealing for 3 h at 700 °C. The open circles are the data points, and the solid line is a four-phase Rietveld refinement. The tick-marks for each refined phase are given below the pattern. The lower trace shows the difference plot (observed–calculated).

Figure 2 shows the diffraction pattern collected after 165 min (∼2.8 h) at 700 °C. Inspection of the data shows the presence of four phases: Cu, Nb, Nb_3Sn, and α-bronze. The open circles are the data points and the solid line is the corresponding four-phase refinement fit. The plot underneath shows the different profile between the observed and calculated peaks, where the range on the y-axis is between -2σ and $+2\sigma$. The parameters obtained from this refinement are given in table 1. Similar refinements were carried out on all diffraction patterns collected at 700, 675, and 660 °C and the weight fraction of Nb_3Sn phase was extracted for all patterns and all temperatures.

The time dependence of the formation of Nb_3Sn during each of the three isothermal anneals is shown in figure 3. The normalized Nb_3Sn weight fractions are shown as a function of time, with $t = 0$ being defined as the time when the sample first stabilized at the required temperature. The solid lines in the figure are fits to the data of the JMAK equation (equation (1)). The time constant, τ, is strongly dependent on annealing temperature, increasing from 3.2 ± 0.5 min at 700 °C to 573 ± 6 min at 660 °C (see table 2). Extrapolation of the fits

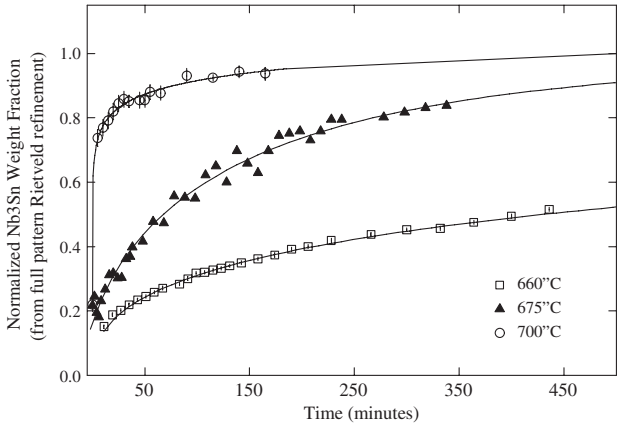

Figure 3. Normalized weight fraction of Nb_3Sn phase in Nb–Sn–Cu wires as a function of time and temperature. The solid lines shown are fits to the JMAK equation (equation (1)).

Table 1. Refined structural parameters for Nb–Sn–Cu wires held at 700 °C for 3 h. U_{ISO} is the isotropic temperature factor; March 1 the March–Dollase coefficient of preferred orientation; $X_{(strain)}$ the coefficient for Lorentzian isotropic strain broadening; and $Y_{(particle)}$ the coefficient for Lorentzian particle size broadening.

	Phase 1 Cu	Phase 2 Nb–2 at.%Ti	Phase 3 Nb_3Sn	Phase 4 Cu–4.9 at.%Sn
Space group	$Fm\bar{3}m$	$Im\bar{3}m$	$Pm\bar{3}n$	$Fm\bar{3}m$
a (Å)	3.668 17(2)	3.3220(3)	5.3242(2)	3.7405(6)
α, β, γ	$\alpha = \beta = \gamma = 90°$	$\alpha = \beta = \gamma = 90°$	$\alpha = \beta = \gamma = 90°$	$\alpha = \beta = \gamma = 90°$
V (Å^3)	49.357(1)	36.662(9)	150.92(2)	52.33(3)
U_{ISO}	0.031(4)	0.031(4)	0.031(4)	0.031(4)
March 1	⟨111⟩2.02(1)			
$X_{(strain)}$		8.83(4)	18.4(2)	
$Y_{(particle)}$	2.56(2)	1.66(2)	1.34(1)	2.46(1)
Weight %	53.3(3)	3.2(2)	32.5(6)	11.1(3)
				$\chi^2 = 5.2$

Table 2. Time constants, τ, from fits to the JMAK equation.

Temperature (°C)	Avrami exponent, n	Time constant, τ (min)
700	0.55(6)	3.2(5)
675	0.66(4)	135(26)
660	0.48(5)	573(6)

indicates that at 700 °C Nb_3Sn phase formation is complete after annealing for ∼8.3 h. At 675 °C complete phase formation would take ∼16.7 h, while at 660 °C it would take ∼166 h (∼7 days) for the Nb_3Sn phase to fully form.

Figure 4 shows all three isothermal phase formation curves plotted in linear form. The data all scale, indicating that a universal growth mechanism governs the formation of Nb_3Sn in the temperature range 660–700 °C. The linearized JMAK equation (equation (2)) provides a good fit to these data with an Avrami coefficient $n = 0.51 \pm 0.01$. A value of $n = 0.5$ is reported

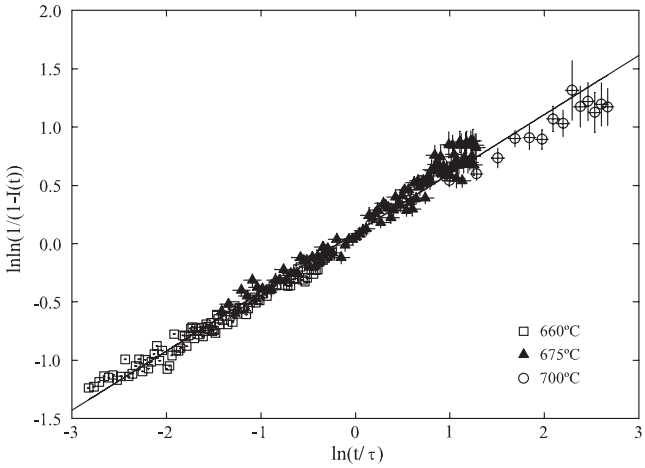

Figure 4. Plot of $\ln(1/(1-I(t)))$ versus $\ln(1/\tau)$ showing scaling in the formation of the Nb_3Sn phase during heating at different temperatures. The solid line is a straight line fit to the linearized JMAK equation with slope $n = 0.51 \pm 0.01$.

as a characteristic of diffusion-controlled phase growth [18, 20]. Although n alone does not give sufficient information to determine the growth mechanism in detail, other workers have reported solid-state diffusion as the driving process during the formation of Nb_3Sn phase in Nb–Sn–Cu internal-Sn wires [21–24] and therefore we believe it is reasonable to suggest that this analysis provides a realistic description of the growth process in Nb_3Sn.

Figure 5 shows the linear relationship between $\ln k$ and $1/k_BT$. If we assume that the rate constants follow the Arrhenius law an apparent activation energy $E_a = 10 \pm 1$ eV (963 ± 97 kJ mol^{-1}) is determined from fitting equation (3) to these data. A value of ~10 eV is higher than might be expected, since most metallic systems have activation energies of phase formation between 2 and 5 eV. However, high values of E_a (>9 eV) have been reported in certain cases; for example, Kuijpers *et al* [25] measured an activation energy of 950 kJ mol^{-1} (9.9 eV) for the transformation of β-AlFeSi to α-Al(FeMn)Si during homogenization, while Schmidt *et al* reported a single activation enthalpy of 12.5 ± 1.0 eV during the crystallization of Si_3N_4/SiC composites from amorphous Si–C–N ceramics [26]. In both cases the phase formation is diffusion controlled, which provides support for our suggestion that Nb_3Sn formation is also a diffusion-controlled process.

It should be possible to separate the activation energy of nucleation (E_{nuc}) and the activation energy of diffusion (E_{diff}) according to the equation given by Kempen *et al* [27]:

$$E_a = \frac{\frac{d}{m}E_{diff} + \left(n - \frac{d}{m}\right)E_{nuc}}{n} \tag{4}$$

where n is the Avrami exponent, d is defined as the dimensionality of growth, and m is the growth mode ($m = 1$ for interface-controlled growth, $m = 2$ for diffusion-controlled growth). Clearly either E_{diff} or E_{nuc} must be explicitly determined in order to derive the other. However, since neither E_{diff} nor E_{nuc} is known in isolation for Nb_3Sn, it has not been possible to separate them in this study.

The grain size of the Nb_3Sn crystallites has been calculated during annealing at 660, 675, and 700 °C using the Scherrer equation:

$$t = \frac{K\lambda}{B\cos\theta} \tag{5}$$

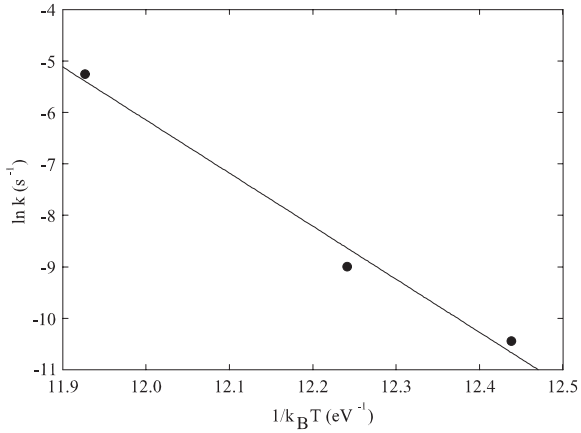

Figure 5. Arrhenius law for the apparent activation energy of nucleation and diffusion-controlled growth of the Nb_3Sn phase. The solid line is the straight-line fit to the data as described in the text.

Table 3. Nb_3Sn grain size after annealing at different temperatures calculated from the Scherrer equation (equation (5)).

Temperature (°C)	Annealing time (h)	Nb_3Sn grain size (Å)
700	3	1390(9)
675	8	780(10)
660	7	810(20)

where t is the grain thickness in Angstroms, K is the Scherrer constant (assumed to be 0.9), λ is the wavelength of neutrons, θ is half the scattering angle, and B is the full width at half maximum (FWHM) of the Bragg peaks. B is calculated using the expression $B^2 = B_S^2 - B_{Si}^2$ where B_S is the FWHM of the sample and B_{Si} is the FWHM of the Si standard. Analysis of grain size using the Scherrer constant of $K \sim 0.9$ assumes that there is very little size distribution in the Nb_3Sn grains. We believe this to be a reasonable assumption based on SEM images by Lee *et al* which show a narrow size distribution of Nb_3Sn grains in internal-Sn Nb_3Sn filaments and generally a uniformity in the Nb_3Sn grain size from filament to filament [6]. The Nb_3Sn grain size for each anneal temperature is given in table 3. In each anneal, once the temperature had stabilized, the grain size did not change appreciably as a function of time. At 660 and 675 °C the grain size was the same (within errors), with a value of ∼800 Å. However annealing at 700 °C increased the grain size by over 70% to 1390 ± 9 Å.

4.2. Implications for Nb_3Sn magnet production industry

Optimizing the rate of Nb_3Sn phase formation and grain size is desirable in order to improve heat treatment processing routes and enhance the overall performance of Nb_3Sn superconducting magnets. Through fitting Nb_3Sn phase formation data to the JMAK model we show that increasing the temperature by 40 °C can decrease the Nb_3Sn formation time from 170 h at 660 °C to ∼7 h at 700 °C. However, this increase in temperature increases the size of the Nb_3Sn grains from ∼800 to ∼1400 Å. Instead, increasing the heat treatment temperature from 660 to 675 °C decreases the Nb_3Sn phase formation time significantly from 170 to 17 h, but does not affect the Nb_3Sn grain size. It should be noted that in the large-scale production of Nb_3Sn magnet coils, annealing for very short periods of time (such as 17 h) is

not practical. This is due to issues of temperature gradients across the large mass of the Nb_3Sn coils, and the temperature ramping and control periods of the large furnaces used. Therefore, we recommended that to optimize the Nb_3Sn heat treatment OIS could increase the stage 3 anneal temperature to 675 °C and reduce the time spent at stage 3 significantly from the current 180 h to a value as close to 17 h as possible within practical consideration limits.

5. Conclusions

By studying Nb_3Sn formation using kinetic neutron diffraction it has been possible to quantify the time and temperature dependence of the rate at which Nb_3Sn forms during the heat treatment of Nb–Sn–Cu wires. The growth mechanism of the Nb_3Sn phase is independent of temperature during isothermal annealing in the range 660–700 °C, and a value of $n = 0.51 \pm 0.01$ indicates diffusion-controlled growth. An apparent activation energy of 10 ± 1 eV for nucleation and diffusion has been found. Our findings reveal that it is possible to reduce the commercial annealing time of stage 3 during the production of Nb_3Sn wires without affecting the size of the Nb_3Sn grains within the superconducting filaments.

Acknowledgments

We would like to thank Professor Bob Cywinski for his invaluable comments and useful discussions. We thank Dr Thomas Hansen (ILL) for his support during the neutron experiment on D20. In addition the authors wish to thank Oxford Instruments Superconductivity for providing samples of precursor Nb–Sn–Cu wire, and funding from the UK's Engineering and Physical Sciences Research Council is gratefully acknowledged.

References

[1] Hense K, Fillunger H, Kajgana I, Kirchmayr H, Lackner R, Maix R K and Müller M 2003 *Fusion Eng. Des.* **66–68** 1103
[2] Barzi E, Gregory E and Pyon T 2001 *IEEE Trans. Appl. Supercond.* **11** 3573
[3] Rodrigues C A, Machado J-P B and Rodrigues D Jr 2003 *IEEE Trans. Appl. Supercond.* **13** 3426
[4] Barzi E and Mattafirri S 2003 *IEEE Trans. Appl. Supercond.* **13** 3414
[5] Mattafirri S, Barzi E, Fineschi F and Rey J-M 2003 *IEEE Trans. Appl. Supercond.* **13** 3418
[6] Lee P J and Larbalestier D C 2001 *IEEE Trans. Appl. Supercond.* **11** 3671
[7] Scanlan R M, Fietz W A and Koch E F 1975 *J. Appl. Phys.* **46** 2244
[8] Kolosov V N and Shevyrev A A 2004 *Inorg. Mater.* **40** 235
[9] Lee P J, Fischer C M, Naus M T, Squitieri A A and Larbalestier D C 2003 *IEEE Trans. Appl. Supercond.* **13** 3422
[10] Verhoeven J D, Efron A, Gibson E D and Cheng C C 1986 *J. Appl. Phys.* **59** 2105
[11] Kolmogorov A N 1937 *Bull. Acad. Sci.* **1** 355
[12] Johnson W and Mehl R 1939 *Trans. Am. Inst. Min. Metal.* **135** 416
[13] Avrami M 1939 *J. Chem. Phys.* **7** 1103
[14] Avrami M 1940 *J. Chem. Phys.* **8** 212
[15] Avrami M 1941 *J. Chem. Phys.* **9** 177
[16] Al-Jawad M, Kilcoyne S H and Manuel P 2004 *Phys. Chem. Glasses* **45** 97
[17] Stewart J R and Cywinski R 1999 *J. Phys.: Condens. Matter* **11** 7095
[18] Christian J W 1981 The theory of transformations in metals and alloys *Materials Science and Technology* (Oxford: Pergamon)
[19] Larson A C and Von Dreele R B 2004 *General Structure Analysis System (GSAS)* Los Alamos National Laboratory Report LAUR 86-748
[20] Pradell T, Crespo D, Clavaguera N and Clavaguera-Mora M T 1998 *J. Phys.: Condens. Matter* **10** 3833
[21] Welsch D O, Dienes G J, Lazareth O W and Hatcher R D 1983 *IEEE Trans. Magn.* **19** 889

[22] Yoshizaki K, Taguchi O, Fujiwara F, Imaizumi M, Wakata M, Hashimoto Y, Wakamoto K, Yamada T and Satow T 1983 *IEEE Trans. Magn.* **19** 1131
[23] Muller H and Schneider T 2004 *Physica* C **401** 325
[24] Tan K S, Hopkins S C, Glowacki B A, Majoros M and Astill D 2004 *Supercond. Sci. Technol.* **17** 663
[25] Kuijpers N C W, Vermolen F J, Vuik C, Koenis P T G, Nilsen K E and van der Zwaag S 2005 *Mater. Sci. Eng.* A **394** 9
[26] Schmidt H, Borchardt G, Müller A and Bill J 2004 *J. Non-Cryst. Solids* **341** 133
[27] Kempen A T W, Sommer F and Mittemeijer J 2002 *J. Mater. Sci.* **37** 1321